Geophysical Research Letters

RESEARCH LETTER
10.1029/2023GL104709

Cause of Substantial Global Mean Sea Level Rise Over 2014–2016

William Llovel[1], Kevin Balem[1], Soumaia Tajouri[1], and Antoine Hochet[1]

[1]Laboratoire d'Océanographie Physique et Spatiale (LOPS), University Brest, CNRS, Ifremer, IRD, IUEM, Plouzané, France

Key Points:

- Global mean sea level rose by 15 mm over June 2014 – May 2016
- 80% of this rise had a mass origin (12 mm) and 20% had an ocean warming origin (3 mm)
- The terrestrial water storage change in the Amazon basin (5 mm) contributed to one third of the substantial sea level rise

Supporting Information:

Supporting Information may be found in the online version of this article.

Correspondence to:

W. Llovel,
william.llovel@ifremer.fr

Citation:

Llovel, W., Balem, K., Tajouri, S., & Hochet, A. (2023). Cause of substantial global mean sea level rise over 2014–2016. *Geophysical Research Letters*, *50*, e2023GL104709. https://doi.org/10.1029/2023GL104709

Received 6 JUN 2023
Accepted 24 SEP 2023

Author Contributions:

Conceptualization: William Llovel
Data curation: Kevin Balem
Investigation: Soumaia Tajouri, Antoine Hochet
Methodology: William Llovel
Software: Kevin Balem
Supervision: William Llovel
Writing – original draft: William Llovel
Writing – review & editing: William Llovel, Kevin Balem, Soumaia Tajouri, Antoine Hochet

Abstract Global mean sea level rose by 15 mm over June 2014 – May 2016. This rise is 7 mm larger than the 8 mm increase associated with the long-term trend of 4 mm/yr estimated over 2006–2016. Using a combination of satellite gravimetry data and in situ measurements, we find that 20% of this rise is explained by ocean thermal expansion and 80% by an ocean mass increase, the latter being largely correlated with an equivalent terrestrial water storage (TWS) decrease. Half of the global ocean mass increase during that period can be attributed to the South American continent where we find a significant contribution of the TWS over the Amazon basin (5 mm). This TWS change between oceans and continents occurred during two El Nino events: one aborted in 2014–2015 and an extreme event in 2015–2016 which affected precipitation patterns, especially over the equatorial Pacific ocean and over South America.

Plain Language Summary Interannual variability of global mean sea level (GMSL) change is linked to natural climate modes of variability such as El Nino Southern Oscillation (ENSO). Over May 2014–June 2016, two consecutive El Nino events (warm phase of ENSO) occurred in the tropical Pacific ocean: one aborted in 2014–2015 and an extreme event in 2015–2016. At the same time, satellite altimetry recorded a GMSL increase of 15 mm. 80% of the rise was due to a global ocean mass increase. Half of the global ocean mass increase is attributed to the South American continent with an exceptional contribution from the Amazon basin (5 mm). Those unusual El Nino events affected the precipitation pattern worldwide, decreasing the TWS in the Amazon basin and therefore leading to an increase of the global mean ocean mass. Our results suggest the importance of TWS changes, especially in the tropics, to explain interannual variability of GMSL recorded by satellite altimetry.

1. Introduction

Sea level rise is a direct consequence of the on-going global warming. Currently, 267 million people worldwide live on land less than 2 m above sea level. By 2,100, with a 1 m sea level rise and zero population growth, that number could increase to 410 million people (Hooijer & Vernimmen, 2021). Thus, investigating sea level change is relevant for future socio-economic impacts. Sea level has been routinely monitored by satellite altimetry since the launch of TopEx/Poseidon in August 1992 and its successors (Jason constellations, ERS1-2, ENVISAT, Saral/Altika, and more recently Sentinel-6 MF; Abdalla et al., 2021) with a nearly global coverage. Those data reveal an increase of the global mean sea level (GMSL) of 3.3 ± 0.3 mm/yr over 1993–2021 (Guérou et al., 2023).

Predicting sea level rise is of great interest and determining the average linear rate of rise is not sufficient. Understanding the mechanisms driving GMSL variability is an important issue and especially how they evolve in time. Interannual variations superimposed on the long-term trend experience changes associated to natural climate modes of variability. It is well established that the El Nino-Southern Oscillation (ENSO) events leave imprints on GMSL change over the past years to decades (Hamlington et al., 2020; Llovel et al., 2011; Piecuch & Quinn, 2016). Sea level rise from thermal expansion and global ocean warming (known as global-mean thermosteric sea level) and global ocean mass increase (known as barystatic sea level, Gregory et al., 2019) are the main drivers of the GMSL rise from seasonal to decadal time scales. The latter increases in response to continental ice melt from ice sheets (from Greenland and Antarctica), mountain glaciers and land water storage change. Therefore, GMSL is closely tied to both Earth energy imbalance and the global water cycle.

Both global-mean thermosteric and barystatic components can now be directly assessed using complementary observing systems. First, the Argo Program has been developed to continuously record the temperature and salinity of the oceans (Roemmich et al., 2019). Since 2005/2006, a nearly global array of about 4,000 profiling floats allows global metrics such as global mean thermosteric sea level change from the sea surface to 2,000 dbar to be

quantified. Subsequently, Gravity Recovery and Climate Experiment (GRACE) satellites have been launched in March 2002 to monitor the Earth's gravity field changes and thus, to track mass movements from the different climate reservoirs (hydrosphere, cryosphere, and oceans, Tapley et al., 2019; Chen et al., 2022). Those complementary observing systems allow the sea level budget from seasonal (Leuliette & Willis, 2011) to interannual (Chambers et al., 2017) and decadal time scales (Llovel et al., 2019) to be assessed, thought the deep ocean contribution below 2,000 dbar is less-well constrained (Llovel et al., 2014).

Barystatic change can be estimated using different approaches based on ocean salinity (Munk, 2003; Ponte et al., 2021) or directly from GRACE data over the oceans or indirectly by assessing land freshwater coming from ice sheets, mountain glaciers and land water storage. The latter is known as the global ocean mass budget approach (Chen et al., 2022). While Greenland, Antarctica and mountain glaciers discharge freshwater into the oceans with low frequency variability (such as trends or acceleration), net land water storage do not experience a strong long term trend but large annual to interannual variability instead (Horwath et al., 2022). Land water is stored in different reservoirs such as rivers, lakes, dams, wetland, root zone, aquifers, and snowpack. Terrestrial waters are continuously exchanged between oceans and atmosphere through vertical and horizontal mass fluxes (precipitations, evaporation, surface runoff and underground flows). Those exchanges contribute to global Earth's energy and mass budgets. Therefore, climate change will ultimately modify terrestrial water storage (TWS).

Global Earth's water cycle is almost balanced at interannual and decadal time scales (Kuo et al., 2021). Thus, to estimate the net contribution of land water storage on GMSL, we can consider the conservation of water mass in the Earth's system. On annual to interannual time scales, the global mass of Earth is conserved:

$$\Delta M_{\text{Oceans}} + \Delta M_{\text{Atmosphere}} + \Delta M_{\text{Land}} = 0 \quad (1)$$

where ΔM represents water mass changes for the three considered reservoirs: oceans, atmosphere and land.

As the time of residence of water in the atmosphere is within 8–10 days (Ent & Tuinenburg, 2017), the atmospheric water mass changes can be neglected on monthly and longer timescales. Therefore, Equation 1 can be written as the balance between ocean water mass changes and TWS mass changes:

$$\Delta M_{\text{Oceans}} = -\Delta M_{\text{Land}} \quad (2)$$

Continental mass changes ΔM_{Land} can be estimated from GRACE data. Note that GRACE records vertically integrated water mass changes so GRACE infers TWS changes which is the sum of snow, ice, surface water, soil moisture and groundwater changes (Tapley et al., 2019).

During the strong La Nina event between the beginning of 2010 and mid 2011 (cold phase of ENSO), the GMSL dropped by 5 mm (Boening et al., 2012). This drop was attributed to an equivalent increase of TWS especially over Australia (Fasullo et al., 2013). Since then, the Southern Oscillation Index (SOI; Figure S1 in Supporting Information S1) -a standardized index measuring the large-scale fluctuations in air pressure occurring over the tropical Pacific Ocean- identified the occurrence of two positive phases of El Nino over 2014–2016. Those events have been described in the literature as an aborted El Nino event in 2014–2015 followed by an extreme El Nino event in 2015–2016 (Levine & McPhaden, 2016) being the strongest El Nino event on record (Zhong et al., 2019). While land water contribution to interannual GMSL change during El Nino and La Nina events has been previously reported in the literature generally (Hamlington et al., 2020; Kuo et al., 2021; Piecuch & Quinn, 2016), it remains to understand the land water contribution to such an unusual El Nino event like this on GMSL change.

This is the purpose of the present study which aims at estimating the GMSL budget. To do so, we will compare the GMSL change inferred from satellite altimetry data to the sum of the different sea level components based on Argo and GRACE data.

The paper is organized as follows. Section 2 will present the data and methods considered in this study. Section 3 will present the results for the GMSL rise of 15 mm during two consecutive El Nino events (June 2014–May 2016). Finally, we will summarize the results, address the broader implications of our main findings and discuss the perspectives motivated by this paper in Section 4.

2. Data and Methods

2.1. Satellite Altimetry Data

We consider in this study the GMSL time series provided by AVISO (https://www.aviso.altimetry.fr/). This product considers the referenced satellite missions (TopEx/Poseidon, Jason-1/-2/-3, and Sentinel-6 MF) from January 1993 to present. Geophysical corrections (ionospheric, wet and dry troposphere, tides, sea state, etc.) have been applied (Ablain et al., 2019). We consider the time series with annual and semi-annual signals included. The time series is corrected for Glacial Isostatic Adjustment (GIA) of −0.3 mm/yr (Peltier, 2004). Our analysis spans from Jan. 2006 to Dec. 2016. The 10-day raw data are used to compute the monthly mean averages. The 10-day satellite altimetry error has been estimated to be 4 mm globally based on tide gauge calibration for Jason-1 and Jason-2 (Leuliette & Willis, 2011). This error becomes 2.6 mm when computing monthly mean estimates assuming that the 10-day altimetric data have an e-folding correlation time of 10 days (Llovel et al., 2014).

2.2. GRACE Data

2.2.1. Global Mean Ocean Mass Time Series

We first make use of global mean ocean mass time series derived from RL06 spherical harmonic coefficients based on GRACE and GRACE-FO missions. We use the solutions computed with Jet Propulsion Laboratory (JPL), Center for Space Research (CSR; Bettadpur, 2018) and GeoForschungsZentrum (GFZ; Dahle et al., 2019) data. The time series represent the ocean mass change only (the global mean atmospheric loading over the oceans has been removed). No Gaussian filter has been applied and a constant 1,023.6 kg/m^3 water density has been considered to convert the gravity mass anomaly to water height. The GIA effect has been corrected with the ICE6G-D model (Peltier et al., 2018). Corrections are also applied for the geocenter (Sun et al., 2016), degree-1 (Swenson et al., 2008), degree-2, and order-0 (C20) (Loomis et al., 2020) coefficients. Based on the three barystatic sea level solutions, we find a Root-Mean Square Error (RMSE) mean of 1.2 mm on a monthly basis.

To assess the reliability of global mean ocean mass change inferred from the spherical harmonic solutions, we also make use of the Mass Concentration (Mascon) solutions provided by the JPL (Watkins et al., 2015), CSR (Save et al., 2016), and Goddard Space Flight Center (GFSC; Loomis et al., 2020). Those solutions consist of using a-priori constraints (in space and time) to estimate monthly gravity fields over equal-area of 3° × 3° spherical caps. Those solutions provide better signal-to-noise ratios compared to the spherical harmonic solutions. In addition to the other geophysical corrections described for the spherical harmonic solutions, the ellipsoidal correction from Ghobadi-Far et al. (2019) has been applied as the spherical cap mascons are placed on a surface of an elliptical Earth. Based on the three mascon solutions, we find a RMSE mean of 1.3 mm on a monthly basis.

2.2.2. Land Grids

To estimate the TWS change, we make use of the RL06 spherical harmonics land grid from CSR, JPL, and GFZ from January 2006 to December 2016 (Landerer, 2021; Landerer & Swenson, 2012). In addition to the corrections made for the ocean grids, a destriping filter and a 300-km Gaussian filter have been applied to the data. The land-grid-scaling is also applied to the spherical harmonic data. As spherical harmonic land grids are not suitable for cryospheric studies, we consider the JPL mascon solution for estimating the ice sheets contribution (Greenland and Antarctica) to net TWS changes in equivalent GMSL.

2.3. Thermosteric Sea Level Data

We consider four different Argo-based gridded products to compute the global mean thermosteric sea level: SCRIPPS (Roemmich & Gilson, 2009); EN4 data from the Met Office Hadley Center (Good et al., 2013); the JAMSTEC MILA GPV (Japan Agency for Marine-Earth Science and Technology Mixed Layer data set of Argo, Grid Point Value) product data (Hosoda et al., 2010) and the ISAS20 data set (Gaillard et al., 2016; Kolodziejczyk et al., 2021). All four data sets are based on Argo data (Argo, 2000), except EN4 data that also includes MBT and XBT data (with the correction of Gouretski & Reseghetti, 2010 applied). All data sets cover the period January 2006 – December 2016.

Ocean salinity changes have second-order effects on GMSL changes (Gregory & Lowe, 2000; Llovel et al., 2019). However, as in situ data coverage is not perfect, density changes associated to salinity should be considered when

data are available (Chambers et al., 2017). Recent studies highlighted the non-closure of the GMSL budget after 2016 (Barnoud et al., 2021; Chen et al., 2020, 2022). Part of this non-closure can be attributed to a significant fraction of Argo floats experiencing a fast salinity drift in near real time profiles (Wong et al., 2023). Although the non-closure occurs right after the 2015–2016 El Nino event, the GMSL change will be assessed using only the Argo-based temperature changes which are not subject to this issue.

Thermosteric sea-level time series are computed by vertically integrating density anomalies (due solely to temperature changes) with respect to a reference density (conservative temperature of 0°C and an absolute salinity of 35.16504 g/kg) at each level using the TEOS10 equation of state from the surface to 2,000 dbar (see Llovel et al., 2013 for more details on the computation). The different products yield a RMSE of 2.4 mm consistent with previous studies (Boening et al., 2012) at a monthly mean basis.

2.4. Data Processing

All curves presented in the study are anomalies with respect to their seasonal cycle (computed as monthly mean over January 2006 – December 2016). As we are interested in interannual variability, all time series are smoothed with a 8-month running mean window to highlight interannual changes. The envelope uncertainty represents one standard deviation unless otherwise stated.

3. Results

We first evaluate the GMSL change over 2006–2016 (black curve in Figure 1, upper panel). GMSL shows a linear rise of 4 mm/yr over 2006–2016 larger than the 3.3 mm/yr over 1993–2021. On top of the linear rise, we confirm large interannual variability especially during ENSO events such as the La Nina with a 5 mm drop in GMSL from March 2010 to May 2011 in agreement with the results reported by Boening et al. (2012). Interestingly, we find an increase of 15 mm between June 2014 and May 2016 in phase with two successive El Nino events. As the GMSL increase is quite important, we investigate the causes of such a rise. The red curve shows the global mean thermosteric sea level and the cyan curve represents the barystatic sea level term (based on the spherical harmonic solutions directly averaged over the oceans).

The sum of the two components agrees well with the observed GMSL rise inferred from satellite altimetry data within the 1-sigma uncertainty (red curve in Figure 1, lower panel) from 2006 to mid 2016. We thus confirm that the global sea level budget is closed over 2006-mid 2016 within the uncertainties. However, at the end of the time period (mid-2016 to the end of 2016), the agreement between the two curves is no longer valid, confirming the non-closure of the GMSL budget previously reported (Barnoud et al., 2021; Chen et al., 2020, 2022).

Over June 2014 – May 2016, we find a significant barystatic sea level contribution of 12 mm corresponding to 80% of the identified rise based on satellite altimetry data. The remaining 3 mm (20%) is attributed to the global mean thermosteric sea level rise. In light of the significant contribution (80%) of the barystatic sea level, we investigate, in what follows, the underlying causes behind this substantial rise.

We estimate the barystatic change using GRACE data directly over the oceans with the spherical harmonic solutions (mean of the 3 centers; black curve in Figure 2 with its gray 1-sigma uncertainty) and with the mascon solutions (mean of the 3 centers; green curve in Figure 2 with its green 1-sigma uncertainty). Then, we also infer the barystatic change from the ocean mass budget approach as the sum of the TWS contribution from spherical harmonics and Greenland plus Antarctica from the mascon solutions, expressed in equivalent sea level change (red curve in Figure 2). We find consistent linear trends of 2.40 mm/yr; 2.15 mm/yr and 2.26 mm/yr for the spherical harmonic solutions, the mascon solutions, and based on the ocean mass budget, respectively. Those estimates are in line with recent investigations on global ocean mass trends (Barnoud et al., 2023). All time series experience large interannual variability. We find that the mean mascon solution experiences smaller interannual variability during ENSO events than the spherical harmonic solutions or based on the ocean mass budget. During the 2010–2011 La Nina event, the barystatic sea level (black curve based on spherical harmonic solutions) shows a decrease of ∼4 mm in line with the sum of the land components (red curve). Contrarily, the mean mascon solution (green curve) displays a smaller decrease of 2 mm. Similar findings are obtained over June 2014 – May 2016 and especially during the extreme El Nino event with an increase of 12 mm for both the barystatic term (black curve based on spherical harmonic solutions) and the sum of all components (red curve) while the mascon-based

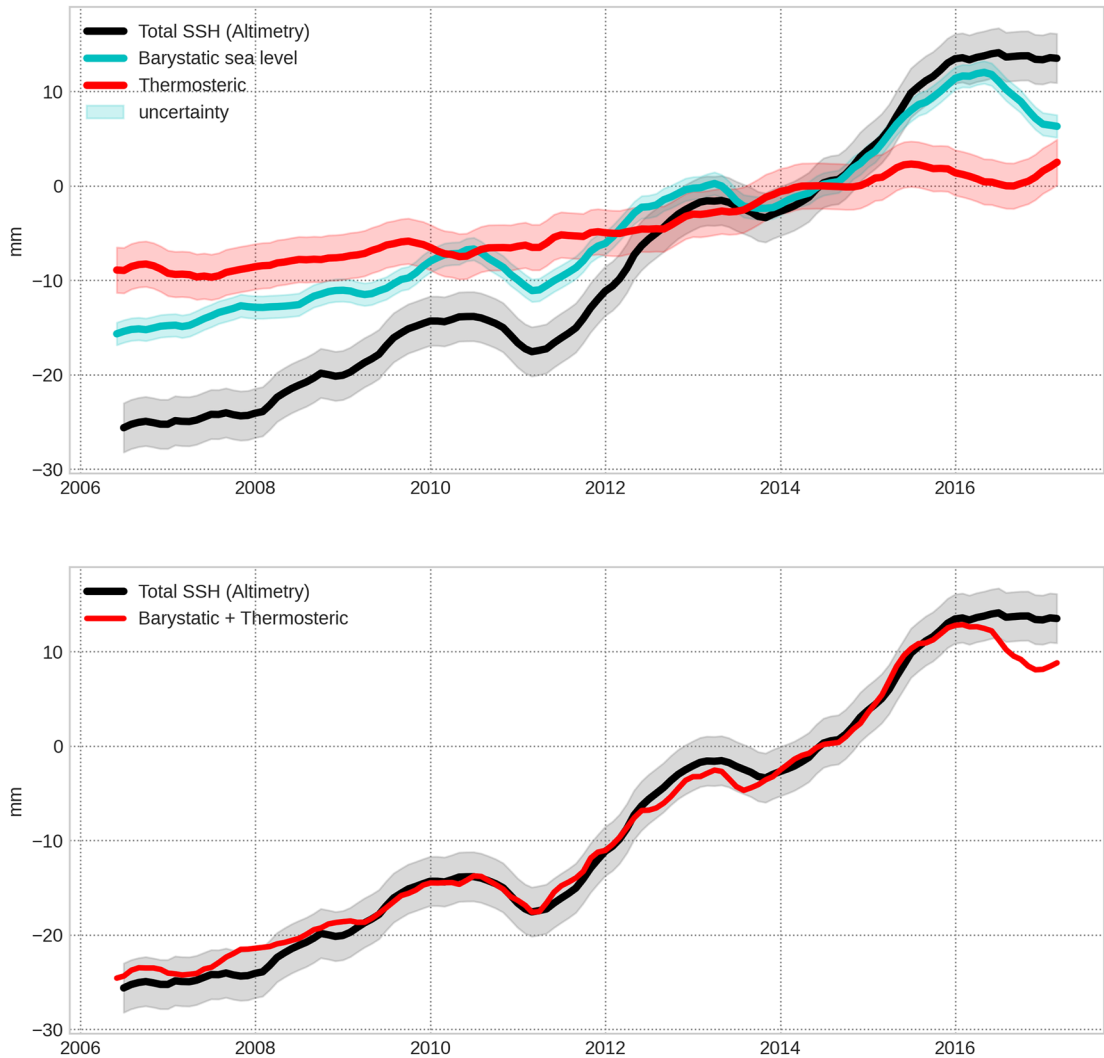

Figure 1. (a) (upper panel) Global mean sea level based on satellite altimetry data (black curve and its 1-sigma gray envelope). Barystatic sea level inferred from Gravity Recovery and Climate Experiment spherical harmonic data (mean of CSR/GFZ/JPL solutions, cyan curve and its 1-sigma envelope of uncertainty). Global mean thermosteric sea level based on Argo gridded products (mean of SIO, EN4, JAMSTEC and ISAS20, red curve and its 1-sigma uncertainty envelope). (b) (lower panel) Sum of barystatic and global mean thermosteric sea level (red curve).

barystatic sea level rise is only 9.2 mm. Our results confirm that the global mass budget is closed over 2006–2016 and we can therefore investigate the contribution of land hydrology to the GMSL change.

Figure 3 presents the barystatic sea level budget assessed over June 2014 – May 2016. The dashed green curve represents the barystatic sea level based on the spherical harmonic solutions from GRACE averaged over the oceans. Solid cyan, pink, brown, light green and orange curves represent the contribution from South America, Africa, Asia/Oceania, Europe, and North America, respectively, in terms of equivalent sea level. The gray solid line represents the contribution of ice sheets (Greenland and Antarctica). The dashed black line represents the sum of the net TWS without the ice sheets' contribution. We highlight that the sum of the world's TWS lies within the 1-sigma envelope uncertainty of the barystatic sea level change suggesting that the TWS plays a significant role over 2014–2016. The land masks used to assess the different contributions are presented in Supporting Information S1 (see Figure S2).

Over June 2014 – May 2016, Greenland and Antarctica ice sheets contributed 1.4 mm (~12%) to the barystatic sea level rise. Africa and Asia/Oceania contributions show a rise reaching 2.5 and 2 mm at the end of 2015, respectively, but decreasing afterward and therefore their contributions are roughly the same as the ice sheets, 1.8 mm (14.8% of the net barystatic sea level rise) and 1.5 mm (12.4% of the net barystatic sea level rise), respectively.

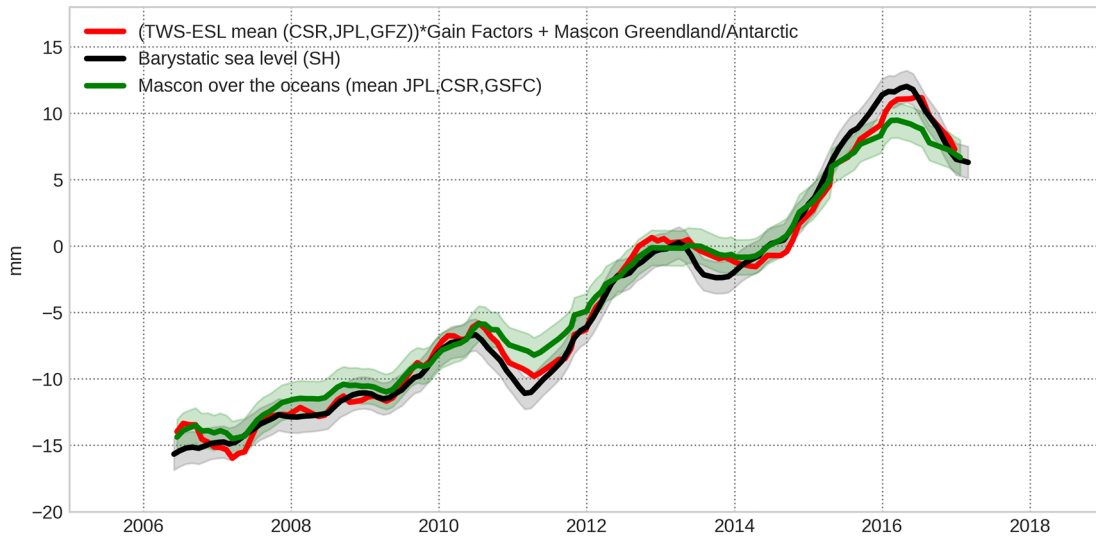

Figure 2. Barystatic sea level change over 2006–2016 inferred directly over the oceans based on Gravity Recovery and Climate Experiment data (spherical harmonics, black curve with its 1-sigma uncertainty). The red curve displays the barystatic sea level due to terrestrial water storage change expressed in equivalent sea level (mean of GRACE-based land grids from CSR/JP/GFZ spherical harmonics) and Greenland plus Antarctica (JPL mascon solution) ice sheets contribution. The green curve represents the barystatic sea level directly computed over the oceans based on the mean of JPL, CSR, and GSFC mascon solutions with its 1-sigma uncertainty (light green envelope).

Interestingly, the net land water storage changes from Africa and Asia/Oceania experience a contribution similar to the mass loss from both ice sheets in terms of equivalent sea level. Europe and North America contributions are very small and account for 0.6 mm (5%) and 0.3 mm (2.5%) of barystatic sea level change. On the other hand, we find a large contribution of 6.2 mm (52% of the barystatic sea level rise) from South America. This rise is not linear and experiences a small increase of 2.5 mm during 2014–2015 and starts to increase at a higher rate afterward to reach 6.2 mm during 2015–2016. Clearly, the ocean mass budget reflects the non-uniform contribution of net land water change from the different parts of the world, especially the large contribution of South America.

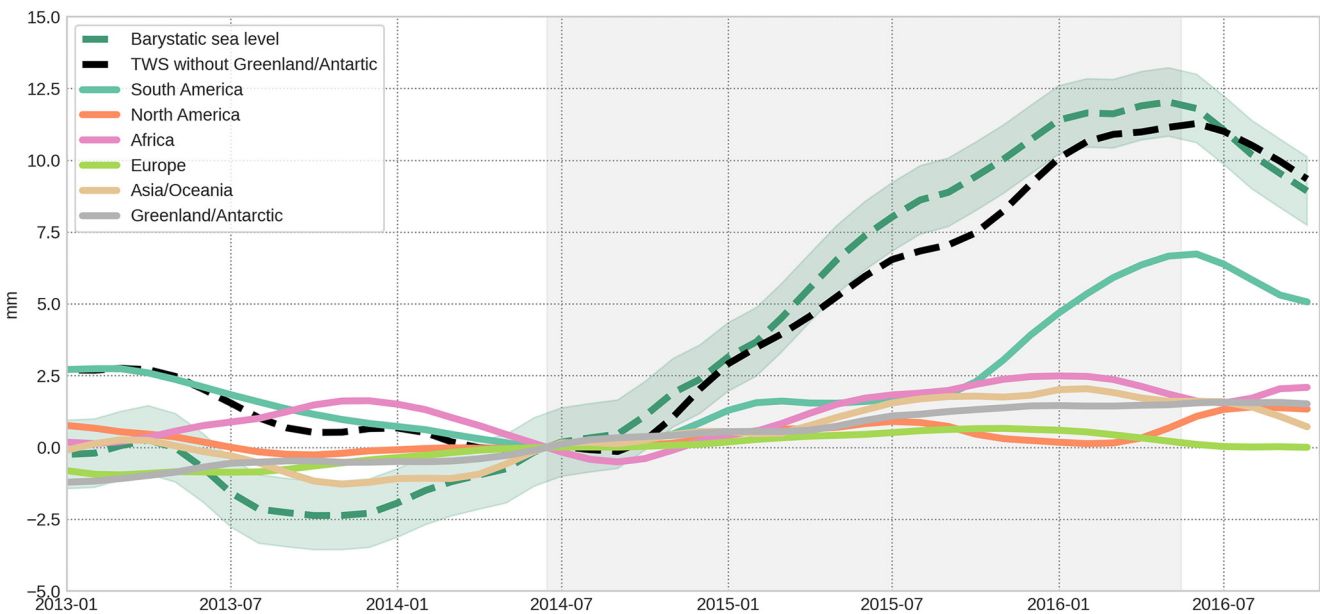

Figure 3. Barystatic sea level budget over June 2014—May 2016. The dash green curve and its 1-sigma envelope represents the barystatic sea level inferred from the spherical harmonics' solutions (terrestrial water storage (TWS) change expressed in equivalent sea level). The solid green curve represents the TWS change for the South American continent. The red curve is the TWS contribution for North America, the pink curve is for Africa, the light green curve is for Europe, the brown curve stands for Asia/Oceania and the gray solid line represents the ice sheets' contribution to sea level.

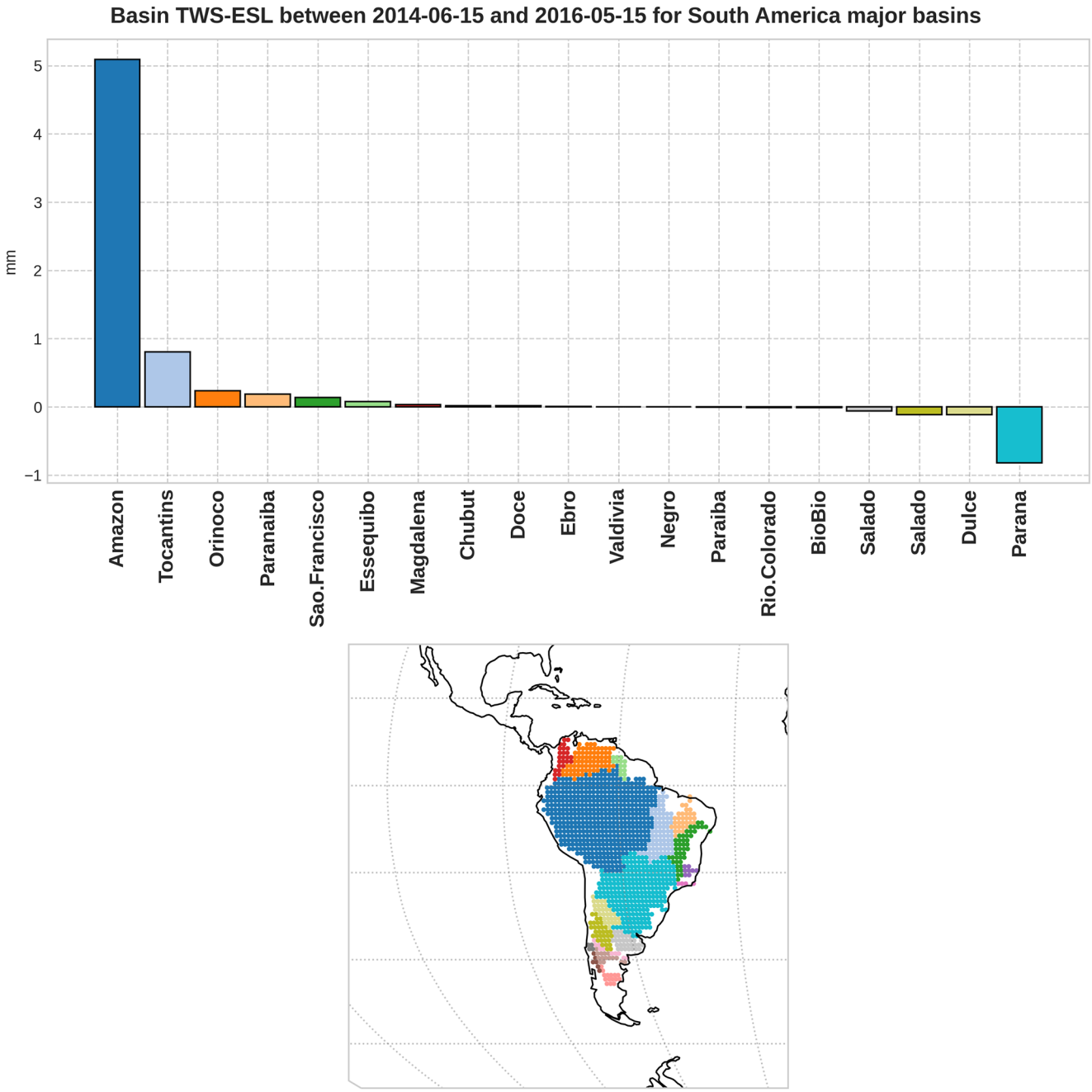

Figure 4. Terrestrial water storage (TWS) change for South America river basins from Gravity Recovery and Climate Experiment (mean estimates based on JPL/CSR/GFZ solutions). TWS change is estimated as the difference between May 2016 minus June 2014. Values are expressed in terms of equivalent sea level (in mm, upper panel). The lower panel shows the location of the 19 river basins: 1. Amazon; 2. Tocantins; 3. Orinocco; 4. Paranaiba; 5. Sao Francisco; 6. Essquibo; 7. Magdalena; 8. Chubut; 9. Doce; 10. Obre; 11. Valdicia; 12. Negro; 13. Paraiba; 14. Rio Colorada; 15. Biobio; 16. Salado1; 17. Salado2; 18 Dulce; 19. Parana.

As South America largely contributes to the barystatic and GMSL rise over the El Nino events, we pursue our analysis in estimating the TWS change over the main hydrologic basins in the South American continent.

To do so, we make use of the Total Runoff Integrating Pathways (TRIP, Oki & Sud, 1998) delimiting the main rivers' basins worldwide. We consider the 19 main rivers' basins in South America (Figure 4). The TRIP masks are provided on a regular grid with a spatial resolution of 0.5°. To apply the masks to the GRACE grids over the continent, we first interpolate the grid onto a regular grid with a spatial resolution of 1° (same spatial resolution as the GRACE-based land grid). Then, we estimate the TWS change for each basin by computing the difference

between June 2014 and May 2016. We clearly find a major contribution from the Amazon basin which accounts for 5 mm in equivalent GMSL change corresponding to 80% of the net TWS change of South America (Figure 4). Then, we find a compensation between a positive contribution from the Tocantins' basin and a negative contribution from the Parana basin (both accounting for less than 1 mm in equivalent sea level). Excluding the Amazon, Tocantins and Parana basins, we find an increase of 1.1 mm over June 2014 – May 2016 in the TWS in South America. Therefore, we find a large contribution of the TWS change in Amazon basin over 2014–2016. The Amazon itself is responsible for ∼42% of the net barystatic sea level rise during the period of interest and ∼33% of the net GMSL rise.

4. Discussion and Conclusions

In this study, we investigate the imprint of two successive El Nino events on GMSL over June 2014 – May 2016. Over June 2014–May 2016, we find an increase of GMSL of 15 mm which is representative of both interannual variability and the long-term trend. Kuo et al. (2021) stated that the extreme 2015–2016 El Nino event caused a rise of 9 mm on the detrended-GMSL (2.5 times larger than the 1997–1998 El Nino recorded by satellite altimetry data) larger than our estimate of 7 mm when removing the 2006–2016 long term trend. The 1997–1998 El Nino was categorized as an Eastern Pacific El Nino event while the 2015–2016 El Nino has been qualified as a combination between an Eastern Pacific event and a Central Pacific event. The latter event contributes to a stronger TWS negative anomaly and subsequently to higher global mean ocean mass increase (Kuo et al., 2021).

We find that the GMSL increase of 15 mm is due to barystatic sea level rise at 80%, the remaining 20% being due to global mean thermosteric sea level rise. Our results confirm that both components are at play during El Nino events. Over 2005–2015, studies have reported that both components contributed to ENSO events equally on average (Hamlington et al., 2020; Piecuch & Quinn, 2016). However, when focusing on particular events, our results suggest that two El-Nino events are not similar. Therefore, this suggests the need to assess the drivers for each ENSO event independently.

By partitioning the TWS changes from the different continents in terms of equivalent GMSL, we find that South America explains half (6.2 mm) of the global ocean mass increase over June 2014 – May 2016. The remainder being due to ice sheet melting, Africa, and Asia/Oceania land water changes and at a second order, North America and Europe. We highlight the large contribution of TWS in the Amazon basin which contributes to increasing the barystatic term and the GMSL by 5 mm over June 2014–May 2016 which accounts for 42% and 33%, respectively.

It is well established that El Nino events leave imprints globally with warmer and wetter conditions over the eastern tropical Pacific ocean, wetter conditions over Argentina and drier conditions over the Amazon region (see Figure 6 in Chen et al., 2022). To confirm this statement, we plotted the map of rain accumulation differences between 2014–2016 and 2012–2014 from the Tropical Rain Measurement Mission (TRMM) precipitation data (Figure S3 in Supporting Information S1, Liu et al., 2012). We find positive anomalies (more rain accumulation) over the central and east tropical Pacific ocean and over Argentina. Negative anomalies corresponding to less precipitation are found in the western tropical Pacific ocean and over the Amazon basin. This confirms an excess of precipitation in the equatorial Pacific ocean and a deficit of precipitation over the Amazon basin.

In a warming climate, El Niño events will likely become more frequent due to climate change within the next two decades regardless of any reduction in carbon emissions (Ying et al., 2022). In addition, projections based on climate models suggest that future El Nino events will be characterized as Central Pacific events which leave larger effects on TWS changes than Eastern Pacific events (Kuo et al., 2021). Therefore, investigating the imprint of past El Nino events on GMSL change and the cause of such rise appears to be highly relevant not only for understanding the physical processes at play but also for assessing the robustness of climate models used to project sea level changes.

Data Availability Statement

GMSL time series can be freely downloaded at https://www.aviso.altimetry.fr/en/data/products/ocean-indicators-products/mean-sea-level/data-acces.html#c12195. GRACE data are available at https://grace.jpl.nasa.gov/data/get-data, supported by the NASA MEaSUREs Program. Land and ocean solutions from CSR, GFZ and JPL are available at

https://doi.org/10.5067/TELND-3AC64
https://doi.org/10.5067/TELND-3AG64
https://doi.org/10.5067/TELND-3AJ64
https://doi.org/10.5067/TEOCN-3AC64
https://doi.org/10.5067/TEOCN-3AG64
https://doi.org/10.5067/TEOCN-3AJ64

The JPL GRACE Mascon Ocean, The JPL GRACE Mascon Ocean, Ice, and Hydrology Equivalent Water Height coastal Resolution Improvement (CRI) Filters RL06 can be download at: https://doi.org/10.5067/TEMSC-3JC63. The CSR GRACE Mascon can be downloaded at: https://www2.csr.utexas.edu/grace/RL06_mascons.html. The GSFC GRACE Mascon can be downloaded at: https://earth.gsfc.nasa.gov/geo/data/grace-mascons. Argo data were collected and made freely available by the International Argo Program and the national programs that contribute to it. The Argo Program is part of the Global Ocean Observing System. The SCRIPPS solution can be downloaded at https://sio-argo.ucsd.edu/RG_Climatology.html. The EN4 data set can be downloaded at https://hadleyserver.metoffice.gov.uk/en4/download-en4-2-2.html. The Japan Agency for Marine-Earth Science and Technology Mixed Layer data set of Argo, Grid Point Value data can be downloaded at https://pubargo.jamstec.go.jp/argo_product/catalog/MOAA_GPV/Glb_PRS/OI/DM/catalog.html and the ISAS20 dataset can be downloaded at https://doi.org/10.17882/52367. The Total Runoff Integrating Pathways (TRIP) have been obtained at http://hydro.iis.u-tokyo.ac.jp/~taikan/TRIPDATA/TRIPDATA.html. TRMM data are freely available at https://disc2.gesdisc.eosdis.nasa.gov/data/TRMM_L3/.

Acknowledgments
William Llovel is supported by the French National Centre for Scientific Research. Kevin Balem is supported by Ifremer. Soumaia Tajouri is supported by a UBO-CNES PhD fellowship. Antoine Hochet is supported by the PACIFIC project from ESA Living Planet Fellowship fundings (grant agreement 4000140684/22/I-DT-lr). This work is supported by the ESA Climate Change Initiative sea-level budget closure (Phase 2) project (grant agreement 4000140620/23/I-NB). The authors acknowledge the Pôle de Calcul et de Données Marines (PCDM) for providing DATARMOR {storage, data access, computational resources, visualization, web-services, consultation, support services}. URL: https://pcdm.ifremer.fr/. We also thank Christopher Piecuch and an anonymous reviewer for their valuable comments and suggestions that help us improve the quality of the paper.

References

Abdalla, S., Abdeh Kolahchi, A., Ablain, M., Adusumilli, S., Aich Bhowmick, S., Alou-Font, E., et al. (2021). Altimetry for the future: Building on 25 years of progress. *Advances in Space Research*, *68*(2), 319–363. https://doi.org/10.1016/j.asr.2021.01.022

Ablain, M., Meyssignac, B., Zawadzki, L., Jugier, R., Ribes, A., Spada, G., et al. (2019). Uncertainty in satellite estimates of global mean sea-level changes, trend and acceleration. *Earth System Science Data*, *11*(3), 1189–1202. https://doi.org/10.5194/essd-11-1189-2019

Argo (2000). Argo float data and metadata from global data assembly centre (Argo GDAC). *SEANOE*. https://doi.org/10.17882/42182

Barnoud, A., Pfeffer, J., Cazenave, A., Fraudeau, R., Rousseau, V., & Ablain, M. (2023). Revisiting the global mean ocean mass budget over 2005–2020. *Ocean Science*, *19*(2), 321–334. https://doi.org/10.5194/os-19-321-2023

Barnoud, A., Pfeffer, J., Guérou, A., Frery, M.-L., Siméon, M., Cazenave, A., et al. (2021). Contributions of altimetry and Argo to non-closure of the global mean sea level budget since 2016. *Geophysical Research Letters*, *48*(14), e2021GL092824. https://doi.org/10.1029/2021GL092824

Bettadpur, S. (2018). *Gravity recovery and climate experiment level-2 gravity field product user handbook*. Tech. Rep. Center for Space Research at The University of Texas at Austin. https://podaac-tools.jpl.nasa.gov/drive/files/allData/grace/docs/L2-UserHandbook_v4.0.pdf

Boening, C., Willis, J. K., Landerer, F. W., Nerem, R. S., & Fasullo, J. (2012). The 2011 La Niña: So strong, the oceans fell. *Geophysical Research Letters*, *39*(19), L19602. https://doi.org/10.1029/2012GL053055

Chambers, D. P., Cazenave, A., Champollion, N., Dieng, H., Llovel, W., Forsberg, R., et al. (2017). Evaluation of the global mean sea level budget between 1993 and 2014. *Surveys in Geophysics*, *38*(1), 309–327. https://doi.org/10.1007/s10712-016-9381-3

Chen, J., Cazenave, A., Dahle, C., Llovel, W., Panet, I., Pfeffer, J., & Moreira, L. (2022). Applications and challenges of GRACE and GRACE follow-on satellite gravimetry. *Surveys in Geophysics*, *43*(1), 305–345. https://doi.org/10.1007/s10712-021-09685-x

Chen, J., Tapley, B., Wilson, C., Cazenave, A., Seo, K.-W., & Kim, J.-S. (2020). Global ocean mass change from GRACE and GRACE Follow-On and altimeter and Argo measurements. *Geophysical Research Letters*, *47*(22), e2020GL090656. https://doi.org/10.1029/2020GL090656

Dahle, C., Murböck, M., Flechtner, F., Dobslaw, H., Micha- lak, G., Neumayer, K., et al. (2019). The GFZ GRACE RL06 monthly gravity field time series: Processing details and quality assessment. *Remote Sensing*, *11*(18), 2116. https://doi.org/10.3390/rs11182116

Ent, R. J., & Tuinenburg, O. A. (2017). The residence time of water in the atmosphere revisited. *Hydrology and Earth System Sciences*, *21*(2), 779–790. https://doi.org/10.5194/hess-21-779-2017

Fasullo, J. T., Boening, C., Landerer, F. W., & Nerem, R. S. (2013). Australia's unique influence on global sea level in 2010–2011. *Geophysical Research Letters*, *40*(16), 4368–4373. https://doi.org/10.1002/grl.50834

Gaillard, F., Thierry, R., Virginie, T., Nicolas, K., & von Karina, S. (2016). In-situ based reanalysis of the global ocean temperature and salinity with ISAS: Variability of the heat content and steric height. *Journal of Climate*, *29*(4), 1305–1323. https://doi.org/10.1175/JCLI-D-15-0028.1

Ghobadi-Far, K., Michal, Š., & Shin-Chan, H. (2019). Determination of ellipsoidal surface mass change from GRACE time-variable gravity data. *Geophysical Journal International*, *219*(1), 248–259. https://doi.org/10.1093/gji/ggz292

Good, S. A., Martin, M. J., & Rayner, N. A. (2013). EN4: Quality controlled ocean temperature and salinity profiles and monthly objective analyses with uncertainty estimates. *Journal of Geophysical Research: Oceans*, *118*(12), 6704–6716. https://doi.org/10.1002/2013JC009067

Gouretski, V., & Reseghetti, F. (2010). On depth and temperature biases in bathythermograph data: Development of a new correction scheme based on analysis of a global ocean database. *Deep-Sea Research I*, *57*, 6–833. https://doi.org/10.1016/j.dsr.2010.03.011

Gregory, J. M., & Lowe, J. A. (2000). Predictions of global and regional sea-level rise using AOGCMs with and without flux adjustment. *Geophysical Research Letters*, *27*(19), 3069–3072. https://doi.org/10.1029/1999gl011228

Gregory, J. M., Griffies, S. M., Hughes, C. W., Lowe, J. A., Church, J. A., Fukimori, I., et al. (2019). Concepts and terminology for sea level: Mean, variability and change, both local and global. *Surveys in Geophysics*, *40*(6), 1251–1289. https://doi.org/10.1007/s10712-019-09525-z

Guérou, A., Meyssignac, B., Prandi, P., Ablain, M., Ribes, A., & Bignalet-Cazalet, F. (2023). Current observed global mean sea level rise and acceleration estimated from satellite altimetry and the associated measurement uncertainty. *Ocean Science*, *19*, 431–451. https://doi.org/10.5194/os-19-431-2023

Hamlington, B. D., Piecuch, C. G., Reager, J. T., Chandanpurkar, H., Frederikse, T., Nerem, R. S., et al. (2020). Origin of interannual variability in global mean sea level. *Proceedings of the National Academy of Sciences of the United States of America*, *117*(25), 13983–13990. https://doi.org/10.1073/pnas.1922190117

Hooijer, A., & Vernimmen, R. (2021). Global LiDAR land elevation data reveal greatest sea-level rise vulnerability in the tropics. *Nature Communications*, *12*(1), 3592. https://doi.org/10.1038/s41467-021-23810-9

Horwath, M., Gutknecht, B. D., Cazenave, A., Palanisamy, H. K., Marti, F., Marzeion, B., et al. (2022). Global sea-level budget and ocean-mass budget, with a focus on advanced data products and uncertainty characterisation. *Earth System Science Data*, *14*(2), 411–447. https://doi.org/10.5194/essd-14-411-2022

Hosoda, S., Ohira, T., Sato, K., & Suga, T. (2010). Improved description of global mixed-layer depth using Argo profiling floats. *Journal of Oceanography*, *66*(6), 773–787. https://doi.org/10.1007/s10872-010-0063-3

Kolodziejczyk, N., Annaig, P.-M., & Gaillard, F. (2021). ISAS temperature and salinity gridded fields. *SEANOE*. https://doi.org/10.17882/52367

Kuo, Y.-N., Lo, M.-H., Liang, Y.-C., Tseng, Y.-H., & Hsu, C.-W. (2021). Terrestrial water storage anomalies emphasize interannual variations in global mean sea level during 1997–1998 and 2015–2016 El Niño events. *Geophysical Research Letters*, *48*(18), e2021GL094104. https://doi.org/10.1029/2021GL094104

Landerer, F. (2021). *TELLUS_GRAC_L3_CSR_RL06_LND_v04. Ver. RL06 v04*. PO.DAAC. https://doi.org/10.5067/TELND-3AC64

Landerer, F. W., & Swenson, S. C. (2012). Accuracy of scaled GRACE terrestrial water storage estimates. *Water Resources Research*, *48*(11), W04531. https://doi.org/10.1029/2011WR011453

Leuliette, E. W., & Willis, J. K. (2011). Balancing the sea level budget. *Oceanography*, *24*(2), 122–129. https://doi.org/10.5670/oceanog.2011.32

Levine, A. F. Z., & McPhaden, M. J. (2016). How the July 2014 easterly wind burst gave the 2015-2016 El Niño a head start. *Geophysical Research Letters*, *43*(12), 6503–6510. https://doi.org/10.1002/2016GL069204

Liu, Z., Ostrenga, D., Teng, W., & Kempler, S. (2012). Tropical rainfall measuring mission (TRMM) precipitation data and services for research and applications. *Bulletin of the American Meteorological Society*, *93*(9), 1317–1325. https://doi.org/10.1175/BAMS-D-11-00152.1

Llovel, W., Becker, M., Cazenave, A., Jevrejeva, S., Alkama, R., Decharme, B., et al. (2011). Terrestrial waters and sea level variations on interannual time scale. *Global and Planetary Change*, *75*(1–2), 76–82. https://doi.org/10.1016/j.gloplacha.2010.10.008

Llovel, W., Fukumori, I., & Meyssignac, B. (2013). Depth-dependent temperature change contributions to global mean thermosteric sea level rise from 1960 to 2010. *Global and Planetary Change*, *101*, 113–118. https://doi.org/10.1016/j.gloplacha.2012.12.011

Llovel, W., Purkey, S., Meyssignac, B., Blazquez, A., Kolodziejczyk, N., & Bamber, J. (2019). Global ocean freshening, ocean mass increase and global mean sea level rise over 2005–2015. *Scientific Reports*, *9*(1), 17717. https://doi.org/10.1038/s41598-019-54239-2

Llovel, W., Willis, J., Landerer, F., & Fukumori, I. (2014). Deep-ocean contribution to sea level and energy budget not detectable over the past decade. *Nature Climate Change*, *4*(11), 1031–1035. https://doi.org/10.1038/nclimate2387

Loomis, B. D., Rachlin, K. E., Wiese, D. N., Landerer, F. W., & Luthcke, S. B. (2020). Replacing GRACE/GRACE-FO C30 with satellite laser ranging: Impacts on Antarctic Ice Sheet mass change. *Geophysical Research Letters*, *47*(3), e2019GL085488. https://doi.org/10.1029/2019GL085488

Munk, W. (2003). Ocean freshening, sea level rising. *Science*, *300*(5628), 2041–2043. https://doi.org/10.1126/science.1085534

Oki, T., & Sud, Y. C. (1998). Design of total runoff integrating pathways (TRIP)—A global river channel network. *Earth Interactions*, *2*(1), 1–37. https://doi.org/10.1175/1087-3562(1998)002<0001:DOTRIP>2.3.CO;2

Peltier, W. (2004). Global glacial isostasy and the surface of the ice-age Earth: The ICE-5G (VM2) Model and GRACE. *Annual Review of Earth and Planetary Sciences*, *32*(1), 111–149. https://doi.org/10.1146/annurev.earth.32.082503.144359

Peltier, W. R., Argus, D. F., & Drummond, R. (2018). Comment on "An Assessment of the ICE-6G_C (VM5a) Glacial Isostatic Adjustment Model" by Purcell et al. *Journal of Geophysical Research: Solid Earth*, *123*(2), 2019–2028. https://doi.org/10.1002/2016JB013844

Piecuch, C. G., & Quinn, K. J. (2016). El Niño, La Niña, and the global sea level budget. *Ocean Science*, *12*(6), 1165–1177. https://doi.org/10.5194/os-12-1165-2016

Ponte, R. M., Sun, Q., Liu, C., & Liang, X. (2021). How salty is the global ocean: Weighing it all or tasting it a sip at a time? *Geophysical Research Letters*, *48*(11), e2021GL092935. https://doi.org/10.1029/2021GL092935

Roemmich, D., Alford, M. H., Claustre, H., Johnson, K., King, B., Moum, J., et al. (2019). On the future of Argo: A global, full-depth, multi-disciplinary array. *Frontiers in Marine Science*, *6*. https://doi.org/10.3389/fmars.2019.00439

Roemmich, D., & Gilson, J. (2009). The 2004–2008 mean and annual cycle of temperature, salinity, and steric height in the global ocean from the Argo Program. *Progress in Oceanography*, *82*(2), 81–100. https://doi.org/10.1016/j.pocean.2009.03.004

Save, H., Bettadpur, S., & Tapley, B. D. (2016). High-resolution CSR GRACE RL05 mascons. *J. Geophys. Res.Solid Earth*, *121*(10), 7547–7569. https://doi.org/10.1002/2016jb013007

Sun, Y., Riva, R., & Ditmar, P. (2016). Optimizing estimates of annual variations and trends in geocenter motion and J2 from a combination of GRACE data and geophysical models. *Journal of Geophysical Research: Solid Earth*, *121*(11), 8352–8370. https://doi.org/10.1002/2016JB013073

Swenson, S., Chambers, D., & Wahr, J. (2008). Estimating geocenter variations from a combination of GRACE and ocean model output. *Journal of Geophysical Research*, *113*(B8), B08410. https://doi.org/10.1029/2007JB005338

Tapley, B. D., Watkins, M. M., Flechtner, F., Reigber, C., Bettadpur, S., Rodell, M., et al. (2019). Contributions of GRACE to understanding climate change. *Nature Climate Change*, *9*(5), 358–369. https://doi.org/10.1038/s41558-019-0456-2

Watkins, M. M., Wiese, D. N., Yuan, D.-N., Boening, C., & Landerer, F. W. (2015). Improved methods for observing Earth's time variable mass distribution with GRACE using spherical cap mascons. *Journal of Geophysical Research: Solid Earth*, *120*(4), 2648–2671. https://doi.org/10.1002/2014JB011547

Wong, A. P. S., Gilson, J., & Cabanes, C. (2023). Argo salinity: Bias and uncertainty evaluation. *Earth System Science Data*, *15*(1), 383–393. https://doi.org/10.5194/essd-15-383-2023

Ying, J., Collins, M., Cai, W., Timmermann, A., Huang, P., Chen, D., & Stein, K. (2022). Emergence of climate change in the tropical Pacific. *Nature Climate Change*, *12*(4), 356–364. https://doi.org/10.1038/s41558-022-01301-z

Zhong, W., Cai, W., Zheng, X.-T., & Yang, S. (2019). Unusual anomaly pattern of the 2015/2016 extreme El Niño induced by the 2014 warm condition. *Geophysical Research Letters*, *46*(24), 14722–14781. https://doi.org/10.1029/2019GL085681